JGR Space Physics

RESEARCH ARTICLE
10.1029/2025JA034298

Evidence for a Localized Burst of Relativistic Electrons Produced in Earth's Plasma Sheet During a Substorm

M. Shumko[1,2], D. L. Turner[1], A. Y. Ukhorskiy[1], I. J. Cohen[1], G. K. Stephens[1], A. Artemyev[3], X. Zhang[4], C. Wilkins[3], E. Tsai[3], C. Gabrielse[5], S. Raptis[1], M. Sitnov[1], and V. Angelopoulos[3]

[1]Johns Hopkins University Applied Physics Laboratory, Laurel, MD, USA, [2]Geophysical Institute, University of Alaska Fairbanks, Fairbanks, AK, USA, [3]Department of Earth, Planetary, and Space Sciences, University of California Los Angeles, Los Angeles, CA, USA, [4]Department of Physics at University of Texas at Dallas, Richardson, TX, USA, [5]The Aerospace Corporation, El Segundo, CA, USA

Abstract Earth's magnetotail and its plasma sheet are highly dynamic, influenced by both the solar wind and the inner magnetosphere. Periodically, energy is explosively released in the magnetotail during substorms. However, the extent to which electrons are accelerated in the magnetotail remains an open question, with recent observations revealing acceleration to energies exceeding all previous theoretical and simulation estimates. Here, we investigate the possible origin and spatial scale of relativistic electron bursts by combining in situ plasma sheet measurements taken by the Magnetospheric Multiscale (MMS) mission, with low Earth orbit electron precipitation measurements taken by the Electron Losses and Fields Investigation (ELFIN). On 17 July 2021 at 19:41 UT, ELFIN detected a transient and intense burst of 3 MeV electrons precipitating into the atmospheric loss cone. These relativistic electrons had energies 10× higher than the surrounding plasma sheet, and had fluxes 10× higher than the nearby Van Allen radiation belt. By comparing the electron spectra between MMS and ELFIN, we suggest the burst originated from the plasma sheet, which is supported by the SST19 magnetic field model. Lastly, MMS did not directly observe the burst, despite observing the central plasma sheet at $r = 17\ R_E$. Altogether, these results suggest that the plasma sheet may be capable of effectively accelerating electrons to relativistic energies over a localized region.

Plain Language Summary Earth's magnetotail, and the plasma sheet embedded in it, is a highly dynamic region that is coupled to both the solar wind, which flows outward from the Sun, and Earth's inner magnetosphere, sculpted by Earth's magnetic field. During substorms, the plasma sheet undergoes explosive reconfiguration of the magnetic fields and particles, which leads to spectacular displays of the aurora. In this paper we use the complementary perspectives from NASA's Magnetospheric Multiscale (MMS) and UCLA's Electron Losses and Fields Investigation (ELFIN). We use these missions to investigate an energetic burst of electrons that was likely generated in the plasma sheet and scattered into Earth's atmosphere on 17 July 2021 at 19:41 UT. This burst contained relativistic electrons with energies 10× higher than in the ambient plasma sheet, and was 10× more intense than the outer Van Allen radiation belt. MMS did not directly observe the burst, despite observing the nearby plasma sheet. These results suggest that the plasma sheet may be capable of effectively accelerating electrons to hazardous energies over a localized region.

Key Points:

- ELFIN observed a burst of 3 MeV electrons possibly originating from Earth's plasma sheet
- MMS, located in the plasma sheet at $r = 17R_E$, did not observe the burst
- The background PS electron spectra were consistent between ELFIN and MMS, in stark contrast to the burst which was significantly harder

Correspondence to:
M. Shumko,
msshumko@gmail.com

Citation:
Shumko, M., Turner, D. L., Ukhorskiy, A. Y., Cohen, I. J., Stephens, G. K., Artemyev, A., et al. (2026). Evidence for a localized burst of relativistic electrons produced in Earth's plasma sheet during a substorm. *Journal of Geophysical Research: Space Physics*, *131*, e2025JA034298. https://doi.org/10.1029/2025JA034298

Received 16 JUN 2025
Accepted 3 APR 2026

Author Contributions:
Conceptualization: M. Shumko, D. L. Turner, A. Y. Ukhorskiy, X. Zhang
Data curation: A. Artemyev, C. Wilkins, E. Tsai, C. Gabrielse, V. Angelopoulos
Formal analysis: G. K. Stephens, S. Raptis, M. Sitnov
Funding acquisition: D. L. Turner, A. Y. Ukhorskiy, I. J. Cohen
Investigation: G. K. Stephens
Methodology: M. Shumko, D. L. Turner, I. J. Cohen, G. K. Stephens, A. Artemyev, X. Zhang, C. Wilkins, E. Tsai, C. Gabrielse, M. Sitnov, V. Angelopoulos
Project administration: D. L. Turner, I. J. Cohen
Resources: V. Angelopoulos
Software: S. Raptis, M. Sitnov, V. Angelopoulos
Supervision: D. L. Turner, A. Y. Ukhorskiy, I. J. Cohen
Validation: A. Artemyev
Visualization: M. Shumko, G. K. Stephens, S. Raptis, M. Sitnov

1. Introduction

Earth's plasma sheet (PS) is a region of hot plasma constrained between oppositely oriented closed field lines in the magnetotail. In its quiescent state, the PS is maintained by a combination of magnetic pressure and tension forces from the lobes, closed field lines in the far magnetotail, and strong fields in the inner magnetosphere. But as the lobe pressure increases from dayside reconnection, during the process known as the Dungey cycle, the PS becomes a reservoir of energy and plasma (e.g., Dungey, 1963; Kivelson & Russell, 1995). During this process the current sheet thins, eventually leading to reconnection and a subsequent cascade of multi-scale phenomena resulting in what is typically called a magnetospheric substorm (e.g., Akasofu, 1964; M. Sitnov et al., 2019). A wide range of subsequent substorm phenomena includes reconnection exhaust jets, flux ropes, bursty bulk flows, injections, and dipolarization fronts (e.g., Gabrielse et al., 2023, and references within). Models show that electrons in these Earthward-flowing structures are heated and accelerated to sub-relativistic (100s keV) energies via the Fermi and the betatron mechanisms (e.g., Birn et al., 2013; Fu et al., 2020; Oka et al., 2023, and references

Writing – original draft: M. Shumko, D. L. Turner, I. J. Cohen, G. K. Stephens, A. Artemyev, C. Gabrielse, S. Raptis
Writing – review & editing: M. Shumko, S. Raptis, M. Sitnov

within). These electrons can then enter the inner magnetosphere, where they seed the ring current and the outer radiation belt (RB) populations (K. A. Sorathia et al., 2018; Turner et al., 2016, 2021).

Over the past few decades, a handful of studies have reported transient bursts of PS electrons up to the instrument's integral energy limits: > 200 keV in Richardson et al. (1993, 1996), > 400 keV in Retzler and Simpson (1969), and > 500 keV by Terasawa and Nishida (1976). More recently, Sun et al. (2025) used the Magnetospheric Multiscale (MMS; Burch et al., 2016) mission to study electrons that were accelerated to 560 keV (also the instrumental upper-energy limit) at a magnetic reconnection site. Since these prior results show energetic electron acceleration up to the instrument's upper-energy limit, the true upper-energy limit is unconstrained. Recently, Zhang et al. (2025) reported electrons up to 3 MeV energies, using two low Earth orbiting (LEO) CubeSat missions: Colorado Inner Radiation Belt Experiment (CIRBE; Li, 2024), and Electron Losses and Fields Investigation (ELFIN; Angelopoulos et al., 2020), and hypothesized their possible PS origin. If confirmed, electron acceleration to several MeV in the PS is much higher than all previous estimates, and thus their origin remains a mystery (Zhang et al., 2025). Closer to the inner magnetosphere, electrons of these energies are observed in the form of transient injections, which are associated with rapid outer radiation belt enhancements (e.g., Gabrielse et al., 2014; Kim et al., 2021; K. Sorathia et al., 2025).

Once accelerated, these relativistic electron bursts are hard to contain in the PS: they either immediately scatter into Earth's atmosphere via magnetic field line curvature scattering (e.g., Sergeev et al., 1983; Wilkins et al., 2023; Zou et al., 2024), or gradient/curvature drift out of the dawn magnetopause in a few minutes (Turner et al., 2021). This is in contrast to the dipolar inner magnetosphere, where multi-MeV electrons are often trapped on closed drift orbits in Earth's outer RB ($4 < r < 8\ R_e$) (Ripoll et al., 2020, and references within).

While Zhang et al. (2025) reported that the PS is capable of accelerating electrons to relativistic and ultra-relativistic energies, their mechanism remains unknown. One way to make progress on understanding their origin is to quantify the scale size of their source region. Are these electrons accelerated simultaneously across the entire PS, or are they accelerated in a spatially localized region such as a reconnection site or a dipolarization front? Prior studies were unable to estimate their size since they used single-point measurements made in the PS (Retzler & Simpson, 1969; Richardson et al., 1993, 1996; Terasawa & Nishida, 1976). Multi-spacecraft observations, supported by advanced methods of reconstruction of magnetic field configuration, are thus need to reveal spatial localization of relativistic electron acceleration region. Zhang et al. (2025) indicated that comparing low-altitude and equatorial measurements may help, but events with a better conjugation should be analyzed to spatially constrain the scale size of the relativistic electron acceleration region in the PS.

In this study we complement Zhang et al. (2025) results with a relativistic PS burst observation during a well-oriented MMS-ELFIN conjunction on 17 July 2021 at 19:41 UT during a moderate substorm. Despite a more ideal conjunction configuration, with MMS observing the central PS at $r = 17\ R_E$, and $\Delta MLT \sim 1$ between MMS and ELFIN, only ELFIN observed the burst. The electron spectra observed by ELFIN Earthward and tailward of the burst was consistent with the MMS spectrum from the central PS, suggesting the PS origin of the burst. We further support this result with the novel SST19 magnetic field model (M. I. Sitnov et al., 2019; Stephens et al., 2019). Finally, we argue that the burst was likely localized in the radial direction, and once accelerated, the remaining eastward-drifting electrons extend azimuthally.

2. Methods

The MMS mission is composed of four identically instrumented satellites launched into a highly elliptical orbit on 13 March 2015 (Burch et al., 2016). The apogee during this observation was near 1 MLT at $r \sim 28\ R_E$ and the orbital period was ~3 days. Each MMS probe contains a suite of wave and plasma instruments and we use the following instruments for characterizing the PS. The thermal and energetic electrons were observed by the Fast Plasma Investigation (FPI; Pollock et al., 2016) and Fly's Eye Electron Proton Spectrometer (FEEPS; Blake et al., 2016), while the low-frequency magnetic fields were observed by the Flux-Gate Magnetometer (FGM; Torbert et al., 2016). We primarily use MMS-1 data since at this time MMS consisted of four closely spaced spacecraft that all observed similar features.

The ELFIN mission was composed of two identical 3U CubeSats launched into a 450 km altitude polar low Earth orbit (LEO) with a 93° inclination, and a 90 min orbit period (Angelopoulos et al., 2020, 2023). They were launched on 15 September 2018 and the mission ended when they disintegrated in the atmosphere in September

2022 (Tsai et al., 2024). Each CubeSat was equipped with an energetic particle detector (EPD) that measured 50 keV–7 MeV electrons in 16 logarithmically spaced energy channels. Also, both CubeSats quantified the instrument's instantaneous pitch angle using the onboard Fluxgate Magnetometer, and they observed the pitch angle distribution by spinning (Tsai et al., 2024). During this event, the spin period was 2.8 s, during which they took 16 measurements. To process the ELFIN-EPD data, we first merged the counts (level 1) and flux (level 2) data products. To ensure sufficient flux statistics, we masked all fluxes that had a corresponding count rate less than 5 counts/sector. Furthermore, to check that ELFIN was spinning properly we discarded spins if the spin-period fell outside the [2.5, 3.5] second range. Next, for each energy channel we averaged the flux in spin-period time intervals, and in [0, 180] degree pitch angles with 20° steps (the approximate ELFIN-EPD field of view). The resulting fluxes are binned in time, pitch angle, and energy. For this event we noticed that ELFIN-EPD neared saturation. To correct for saturation effects, the ELFIN instrument team developed a flux correction algorithm and produced corrected fluxes which we use here, and briefly discuss in Appendix A.

To calculate the omnidirectional flux (j) we simply averaged over the binned pitch angles. And to quantify the strength of the scattering, we calculated the ratio of the precipitating to trapped fluxes $\left(j_{\parallel}/j_{\perp}\right)$. For each time stamp we averaged all fluxes corresponding to pitch angles inside the loss-cone and between the loss- and anti loss-cone angles. The loss cone angle for particles with a mirror point below 100 km altitudes is a standard level 2 data product calculated using the International Geomagnetic Reference Field (IGRF; Alken et al., 2021) magnetic field model and is approximately 60° in LEO. A ratio $j_{\parallel}/j_{\perp} \ll 1$ indicates an empty loss cone, while $j_{\parallel}/j_{\perp} \sim 1$ indicates a full loss cone. The energy-dependent $j_{\parallel}/j_{\perp}$ ratio is an invaluable tool to distinguish different plasma populations and scattering mechanisms originating from regions spanning the inner magnetosphere and magnetotail within each five-minute pass (Angelopoulos et al., 2023; Artemyev et al., 2021, 2022; Wilkins et al., 2023; Zhang et al., 2022).

3. Results

During a small substorm on 17 July 2021, the ELFIN CubeSats traversed the high-latitude region twice between 19:40 and 20:06 UT. During this time period MMS was effectively stationary at $r = 17\ R_E$. The minimum SuperMAG lower electrojet (SML) index (Gjerloev, 2009), a proxy of the lower auroral electrojet (AL) index, reached −225 nT during this substorm.

Figure 1 shows the ELFIN-B and -A electron data from two high-latitude passes 15 min apart at 1.5 MLT. Figures 1a1 and 1a2 show the omnidirectional j; Figures 1b1 and 1b2 show the pitch angles that ELFIN sampled during their spin, with the loss cone and anti-loss cone angles annotated; and Figures 1c1 and 1c2 show the $j_{\parallel}/j_{\perp}$ ratio. Figure 1a1 shows two times where the omnidirectional fluxes reached relativistic (> 500 keV) energies: between 19:42 and 19:44 corresponding to the outer RB footprints, and at 19:41 UT corresponding to higher latitude precipitation. Figure 1c1 also shows that the two regions were characterized by isotropic, or nearly isotropic electron fluxes. At 19:41 UT, ELFIN-B observed a 10-s long burst of < 3 MeV electrons. We indicate this burst with the orange "X" and orange horizontal line in Figure 1a1. This burst was embedded in a region of < 200 keV electron precipitation, and it is the focus of this study.

We characterize the various precipitation regions that ELFIN-B observed using the electron spectra. Figure 1d1 shows three ELFIN electron spectra, represented by the colored lines, that were averaged over time intervals indicated by the color-coded and marked horizontal lines in Figure 1a1. The error bars represent the inter-quartile range of the fluxes at each energy. To quantify these spectra, we fit the flux to an exponential of the form $j(E) = j_0 e^{-E/E_0}$ in the energy range overlapping with MMS-FEEPS. The spectra observed immediately tailward and Earthward of the burst (before and after the burst in the time series) had a similar E-folding energy $E_0 = 35$ keV, while the burst spectrum had an $E_0 = 134$ keV.

Fifteen minutes later, Figures 1a2–1c2 shows that ELFIN-A passed through the same high-latitude region while it also observed the isotropic PS precipitation between 20:01:30 and 20:03:00. However, despite it being in the same local time of as ELFIN-B, ELFIN-A did not observe the burst and the electron spectrum returned to $E_0 = 38$ keV. The absence of the burst, together with the softer spectrum, indicates that the electron scattering mechanisms operating in the PS subsided within 15 min between the two ELFIN passes.

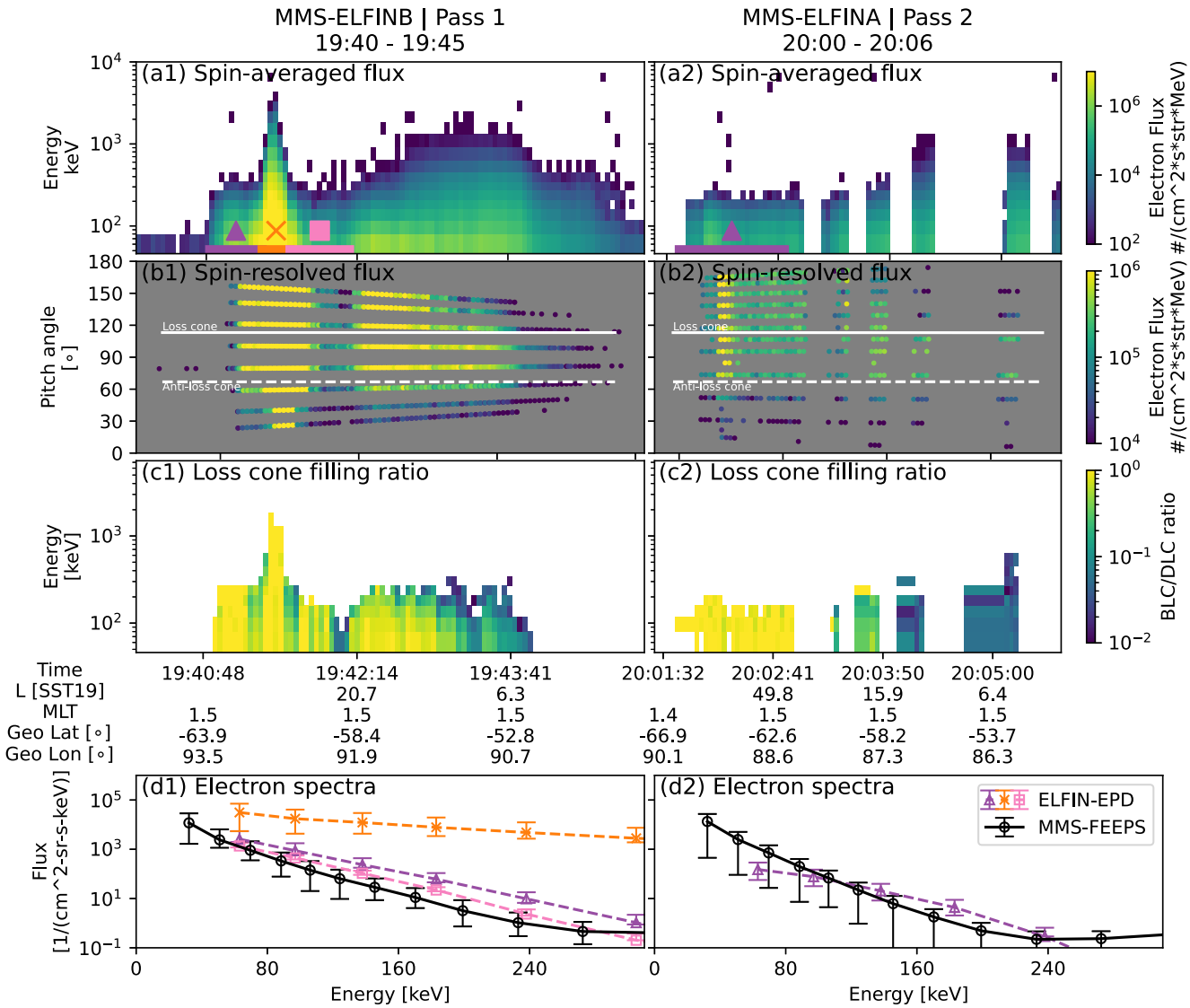

Figure 1. Electron spectra during the two ELFIN passes. Panels (a1) and (a2) show omnidirectional electron flux observed by ELFIN. In about 5 min ELFIN observes the night side magnetosphere from the plasma sheet (PS) to the radiation belt (RB). Only fluxes that correspond to > 5 counts are plotted. This count threshold, together with missing data, corresponds to the white bins. Panels (b1) and (b2) show the 63 keV flux as a function of pitch angle and time, showing how far into the loss cone ELFIN sampled. Panels (c1) and (c2) show the $j_{\parallel}/j_{\perp}$ ratio with yellow indicating a full loss cone. Lastly, panels (d1) and (d2) show the average electron spectrum from MMS-FEEPS and ELFIN. The solid black line with points shows the omnidirectional FEEPS spectrum averaged over each of the 5 min passes. The dashed colored lines are the ELFIN energy spectra taken from the PS region, highlighted with the corresponding colored time spans and markers in Panels (a1) and (a2). The error bars represent the inter-quartile range of the fluxes at each energy.

For the PS perspective, Figure 2 shows the MMS-1 data taken during the two ELFIN passes. At this time MMS was at $\vec{r}_{GSM} = (-16, -2, 5)$ R_E and $MLT = 0.4$ (ΔMLT $= 1.1$ westward of ELFIN). The two sets of red shaded rectangles spanning Figure 2 correspond to the times of the ELFIN passes. Figure 2a shows that MMS was near the central PS during these two time intervals $(|B_x| \sim 0$ nT$)$. In addition, Figure 2a shows highly variable B_z variations indicative of dipolarizing flux bundles. Figures 2b and 2c show the bulk ion velocity in both Geocentric Solar Magnetospheric (GSM) coordinates and projected onto $\vec{B}$. The $v_{\parallel}$ enhancements in between 19:35 and 19:45 are indicative of field-aligned flows in the PS boundary layer, while the $v_{\perp}$ enhancements in between 19:45 and 19:50 are indicative bursty bulk flows in the central PS with velocities reaching 500 km/s. Lastly, Figures 2d and 2e show the high- and low-energy electrons, respectively. The electron fluxes peaked in the 1–10 keV range, and extended to 200 keV energies in the central PS.

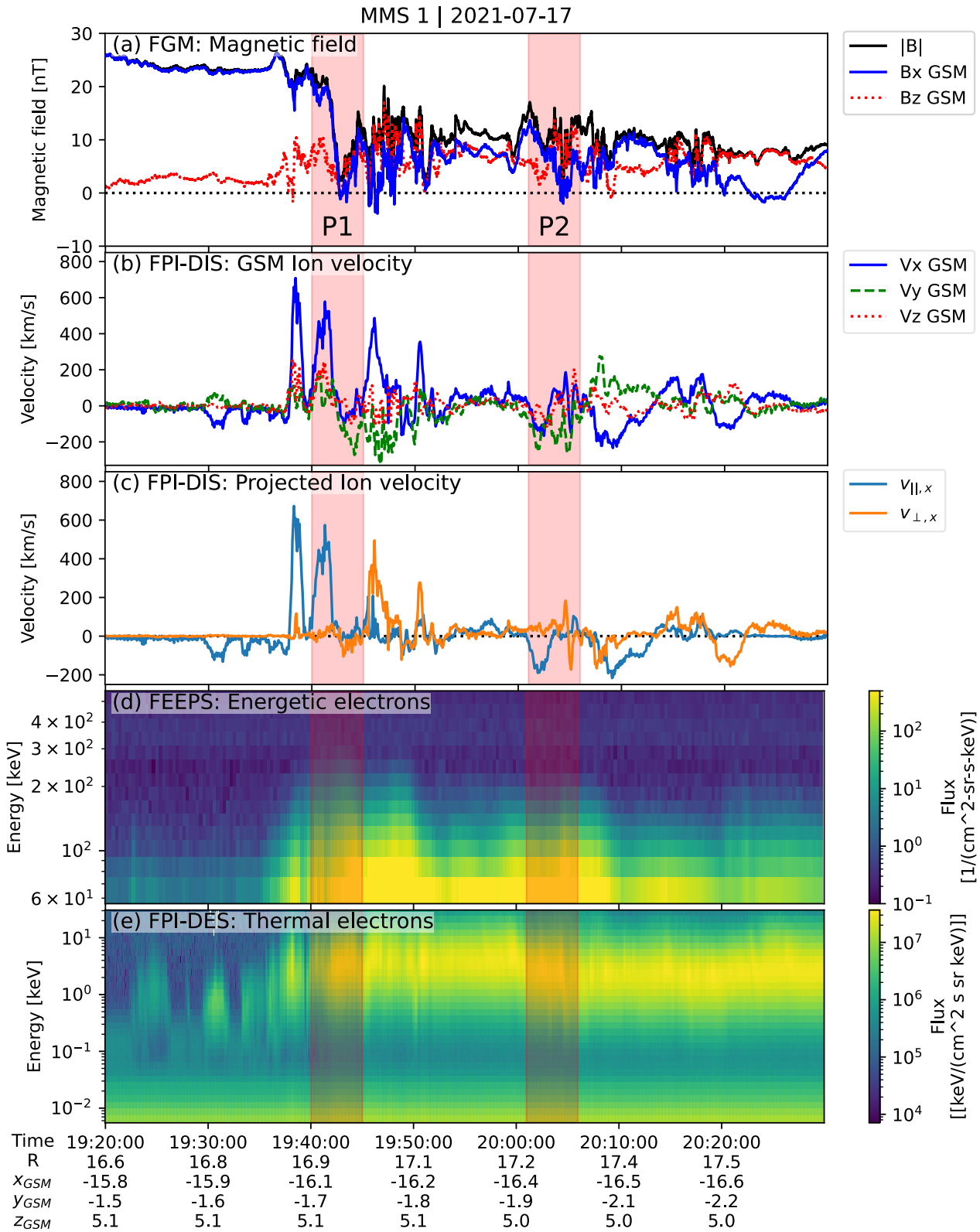

Figure 2. MMS-1 observations taken during ELFIN passes 1 and 2. Panel (a) shows the $|B|$, B_x and B_z magnetic field components. Panels (b) and (c) show the ion velocity in GSM coordinates, and projected to the directions parallel and perpendicular to the magnetic field. Panels (d) and (e) show the energetic and thermal electrons. The time range of the semi-transparent red box spanning all panels corresponds to the two ELFIN passes in Figure 1.

Are the < 200 keV electrons that MMS observed in the PS the same electrons that ELFIN-B observed in Figure 1a1? To address this question we use the fact that in the PS, magnetic field line curvature scattering isotropizes high-altitude fluxes, leading to comparable electron energy spectra at low-altitudes (Artemyev et al., 2022). Similarly to ELFIN, we averaged the MMS energetic electron spectrum over time intervals indicated by the two semi-transparent rectangles in Figure 2d and fit the averaged fluxes with an exponential. The black lines in Figures 1d1 and 1d2 show the resulting MMS high-energy spectra that had an $E_0 = 20$ keV during the two time periods. To check how sensitive our fits are to fitting to a different energy channel range, and to more closely align the lower-energy limit to ELFIN-EPD, we also fit the FEEPS electron spectra to $50 < E < 240$ keV energies and found similar values of $E_0 = 24$ and 19 keV for Passes 1 and 2, respectively.

During Pass 1, the ELFIN fluxes and E_0 spectra observed at latitudes mapping tailward and Earthward of the burst (purple and pink lines) agree within uncertainty with the MMS PS spectrum. Likewise, during Pass 2 the MMS and ELFIN spectra agreed. In stark contrast, however, was the ELFIN burst spectrum (orange line) which exceeded the MMS spectrum by multiple orders of magnitude. With the exception of the burst spectrum, the agreement of the other ELFIN spectra with the MMS PS spectrum during the two passes in Figures 1d1 and 1d2 suggests that the two missions observed the same plasma population. Returning to the burst spectrum, its omnidirectional flux in Figure 1a1 was more than 10× higher than the outer RB flux, and the upper-energy limit of the burst was also 10× higher than the PS it was embedded in.

4. Discussion and Conclusions

While MMS was relatively stationary it observed transient substorm dynamics that were consistent with dipolarizing flux bundles and bursty bulk flows. Concurrently, ELFIN observed the burst of relativistic electrons, the PS, and the outer radiation belt as it passed through field lines which map to those regions. During Pass 1, the LEO precipitating spectra that mapped Earthward and tailward of the burst (the purple and pink lines in Figure 1d1), agree within uncertainty with the central PS spectrum observed by MMS (Artemyev et al., 2022, 2023). The similarity of the < 200 keV PS electron spectra that ELFIN and MMS observed, and the starkly different burst spectrum that ELFIN observed at 19:41 suggests that (a) the source of the burst was embedded in the PS, and (b) MMS was not near the source of the burst.

The former point implies that this acceleration and scattering mechanism was well-separated from the outer RB, which excludes outward radial diffusion as the source of those electrons (Lejosne & Kollmann, 2020, and references within). We support our conclusion using the SST19 magnetic field model that we show in Figure 3 (M. I. Sitnov et al., 2019; Stephens et al., 2019). This novel model has been successfully used to model substorm dynamics, similar to the conditions in this study. SST19 utilizes a flexible model architecture to resolve the magnetic field generated by the primary magnetospheric current systems. This architecture is fit to a subset of magnetometer records mined from a historical archive of space magnetometer data spanning 1995–2023, whose locations are represented by the gray points in Figure 3c. The data mining algorithm, based on the k-nearest neighbor (kNN) method, characterizes the state of the magnetosphere using geomagnetic indices that we show in Figures 3a and 3b, including the SuperMAG (Gjerloev, 2009) pressure-corrected storm (*SMRc*) and substorm (*SML*) indices, their time derivatives, and the solar wind electric parameter vB_z^{IMF} (where v is the solar wind speed and B_z^{IMF} is the z component of the interplanetary magnetic field in the GSM coordinate system). SST19 was customized for use in this study by adding ARTEMIS (Angelopoulos, 2010) magnetometer data to extend its spatial domain to cislunar distances.

Figures 3c and 3d shows the mapped equatorial ELFIN track and MMS location overplotted against the SST19 reconstructed magnetic field between 19:40 and 19:45. MMS was effectively stationary on these time scales while ELFIN traversed field lines that mapped throughout the inner magnetosphere and the PS. The burst, which ELFIN observed over 10 s at 19:41 UT, mapped to distances spanning $33 < r < 36$ R_E down tail. While all magnetic field models are uncertain, especially at those distances, Shi et al. (2024) demonstrated that SST19 accurately predicts the transition between stretched and dipolar field lines which is nominally between geosynchronous and ~ 10 R_E down tail (Donovan, 2016). Therefore, since SST19 mapped the burst $\sim 10s$ of R_E tailward of this transition, this suggests that the origin of the burst was in the PS and not the outer RB.

MMS observed the PS at $r = 17$ R_E, $\Delta MLT \sim 1$ away from ELFIN, yet it did not observe the burst. This implies that the burst likely originated from somewhere along field lines that threaded the PS but not at MMS, and with

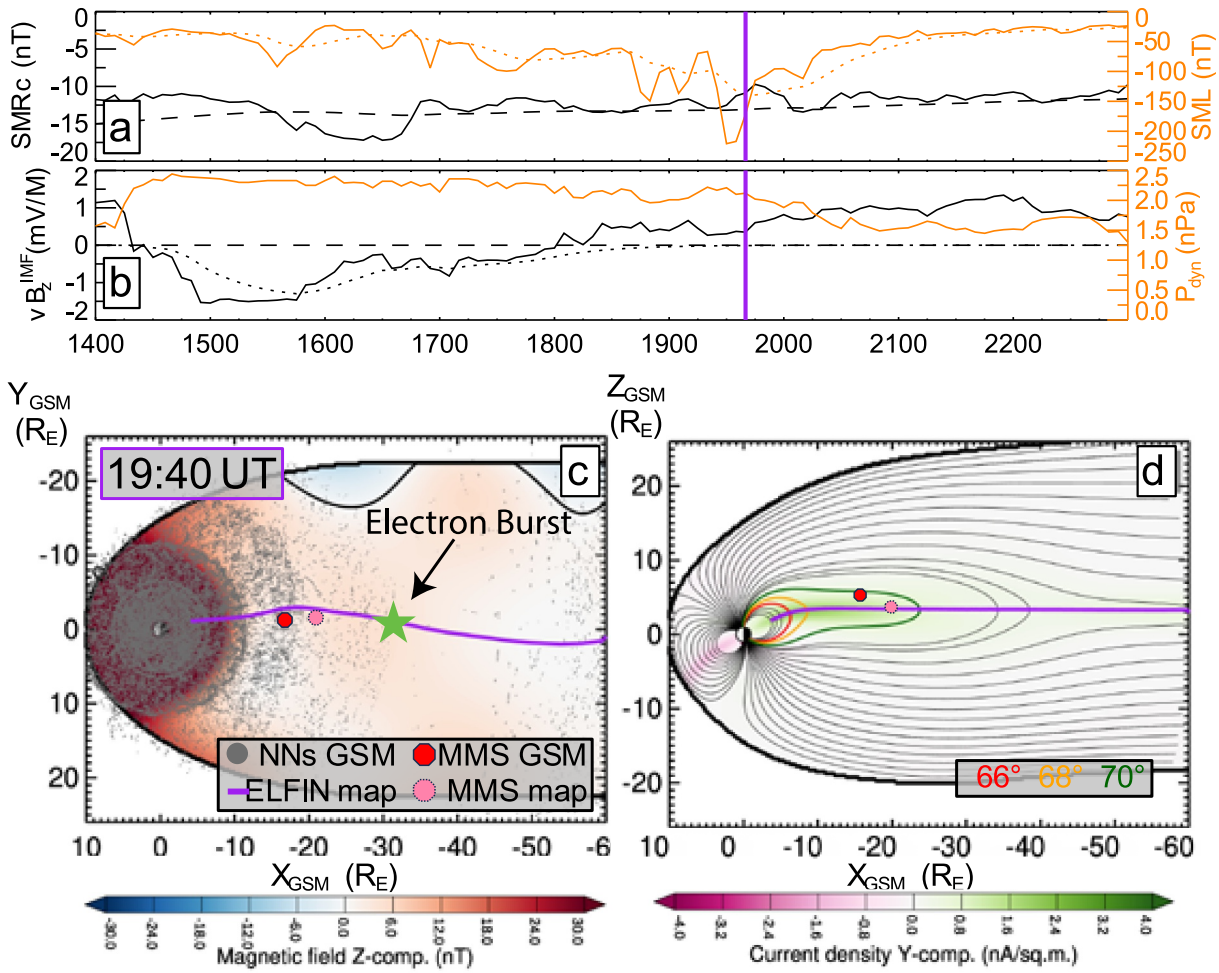

Figure 3. The mapped locations of MMS and ELFIN in the SST19 reconstructed magnetic field. Panel (a) shows the pressure-corrected storm, *SMRc* (black line), and lower substorm electrojet, *SML* (orange line) geomagnetic indices. Their smoothed values, the inputs to SST19, are indicated by the dashed and dotted lines, respectively. Panel (b) shows the solar wind electric field parameter, vB_z^{IMF} (black line), and the dynamic pressure, P_{dyn} (orange line). The smoothed vB_s^{IMF}, an SST19 input, is shown as the dotted black line. The vertical purple line across Panels (a)–(b) is at the time of the conjunction. Panel (c) shows the modeled B_z component in the Y-X plane. The gray dots are the nearest-neighbor (NN) locations of the subset of the historical magnetometer measurements for the SST19 reconstruction. The red and pink circles are at the actual MMS locations (in GSM coordinates), as well as the MMS location mapped to the neutral sheet. The purple line is the mapped ELFIN trajectory during pass 1. Panel (d) show the magnetic field lines in the Z-X plane. The green star in Panel (c) shows the location of the PS burst that mapped to ∼35 R_E.

mapping uncertainties the burst could have potentially originated at a different local time than MMS. Despite these uncertainties, we ascertain that the size of the electron burst was not global, as would be the case if it was of solar origin such as a solar energetic particle event (e.g., Halford et al., 2016).

While can't directly measure the burst's size with the available observatories, we can deduce its azimuthal and radial scale sizes. Since ELFIN observed the burst over a narrow latitude range, it suggests a corresponding narrow radial size of the burst in the PS. This is supported by the SST19 model which predicts a ∼3 R_E radial burst scale size. This estimated radial scale size is larger than estimated by Zhang et al. (2025), but this is unsurprising considering the mapping uncertainties. As for the azimuthal scale size, Turner et al. (2021) suggests that the relativistic PS electrons, which are not immediately scattered into Earth's atmosphere, would azimuthally drift from their source until they escape through the dawnside magnetopause. These electrons would escape in mere minutes, likely before they are transported to the inner magnetosphere by transient phenomena such as bursty bulk flows and dipolarizing flux bundles (e.g., Gabrielse et al., 2023; K. Sorathia et al., 2021; Ukhorskiy et al., 2022; Wiltberger et al., 2015). Thus, in the PS those electrons would be azimuthally extended. Taken together, the aforementioned data and arguments suggest that the burst electrons were radially localized and

azimuthally extended. Since MMS did not observe the burst at $r = 17\ R_E$, this implies that the burst origin was Earthward or tailward of it, with the SST19 model suggesting tailward.

These scale sizes are consistent with Zhang et al. (2025), who surveyed a dozen comparable events in the multi-year ELFIN and CIRBE data sets, underscoring that these phenomena occur far more often than previously assumed. The authors suggested that these electrons were initially accelerated by an X-line which provided $\sim 10 - 100$ keV seed population which was then adiabatically or quasi-adiabatically accelerated by Earthward transport inside plasma flows. During Earthward transport particles experience both an increased magnetic field strength and shorter magnetic field lines, leading to betatron and Fermi acceleration, respectively (Birn et al., 2013, 2014; Fu et al., 2020; Oka et al., 2023, and references within). Therefore, any Earthward transport would lead to some particle acceleration, which can be as large as 10× (Birn et al., 2014; K. A. Sorathia et al., 2018). In addition to adiabatic acceleration, electrons can also be accelerated by waves such as lower hybrid waves, Langmuir waves, electrostatic solitary waves, kinetic Alfvén waves, and whistler mode waves (Khotyaintsev et al., 2019). However, these wave-particle interactions are highly energy-dependent, and none of the wave modes have been shown to directly accelerate electrons to relativistic energies in the magnetotail (e.g., Chepuri et al., 2023). Notwithstanding the lack of evidence, the contribution of wave-particle interactions should be further investigated. This can be addressed in future studies by identifying these bursts directly in the PS, and quantifying trends in the local field and the particle environment. These observations should be complemented by MHD simulations with particle transport and self-consistent wave-particle interactions.

We now place this PS burst in the context of historical LEO observations. Brown and Stone (1972) studied relativistic precipitation observed by the Ogo 4 satellite that orbited in LEO, and what they call "Type 2" and "Type 3" events appear similar to the PS burst event analyzed here. The authors hypothesized, similarly to Zhang et al. (2025), that "Type 2" events were a result of magnetic reconnection. Furthermore, the appearance of this burst in a time series shares similarities with precipitation bands that were observed by the Solar Anomalous and Magnetospheric Particle Explorer (SAMPEX; Baker et al., 1993), although most precipitation bands were associated with the outer radiation belt (Blake et al., 1996; Blum et al., 2015). However, prior observations had insufficient energy resolution and pitch angle coverage that is necessary to unambiguously identify burst of electrons originating from the PS.

In summary, combining high- and low-altitude observations taken by MMS and ELFIN enabled an unprecedented view of relativistic electrons which were likely accelerated in, and scattered from, Earth's PS. The electron burst fluxes were least 10× more intense than the outer RB, and we hypothesize that it originated from the PS, with a 3 MeV upper-energy limit which was 10× higher than the PS it was embedded in. Despite direct PS observations made by MMS ∼1 hour away in local time from ELFIN, it did not observe the burst, hinting that the burst was localized to only a part of the PS. The burst's narrow latitude extent implies a localized radial extent on an order of an R_E. And since the remaining electrons drift eastward, this suggests that after the original burst was accelerated and scattered, the remaining electrons would extend azimuthally. All in all, the complementary low- and high-altitude observations from ELFIN and MMS suggests that Earth's plasma sheet can efficiently accelerate electrons up to 3 MeV energies—and scatter them into the atmosphere—in a region that is radially localized and is tailward of the inner-edge of the plasma sheet.

Appendix A: ELFIN Electron Spectrum and Saturation

When calculating the electron energy spectrum from ELFIN-EPD, we should be mindful of the instrument saturation. The burst studied here pushed the instrument to the brink of saturation—evident for times when the total count rate from all channels exceeds 10^5 counts/second. Figure A1a shows the electron counts, summed over all energy channels. We indicate the times when the total count rates approached 10^5 counts/second with the vertical magenta lines. When saturated, the instrument underestimates fluxes. Thus, the ELFIN instrument team reconstructed the true fluxes assuming the paralyzable-type detector model (Usman & Patil, 2018). This model includes the specific detector coincidence logic of the ELFIN-EPD, where counts measured in the high energy channels could override counts that were being simultaneously processed in the lower energy channels, if they were observed within the rise time window (nominally 2.4 μs) of the shaped pulse provided by the preamplifiers. As a result, the counts in a particular energy channel are affected by the sum of the counts in the higher energy channels.

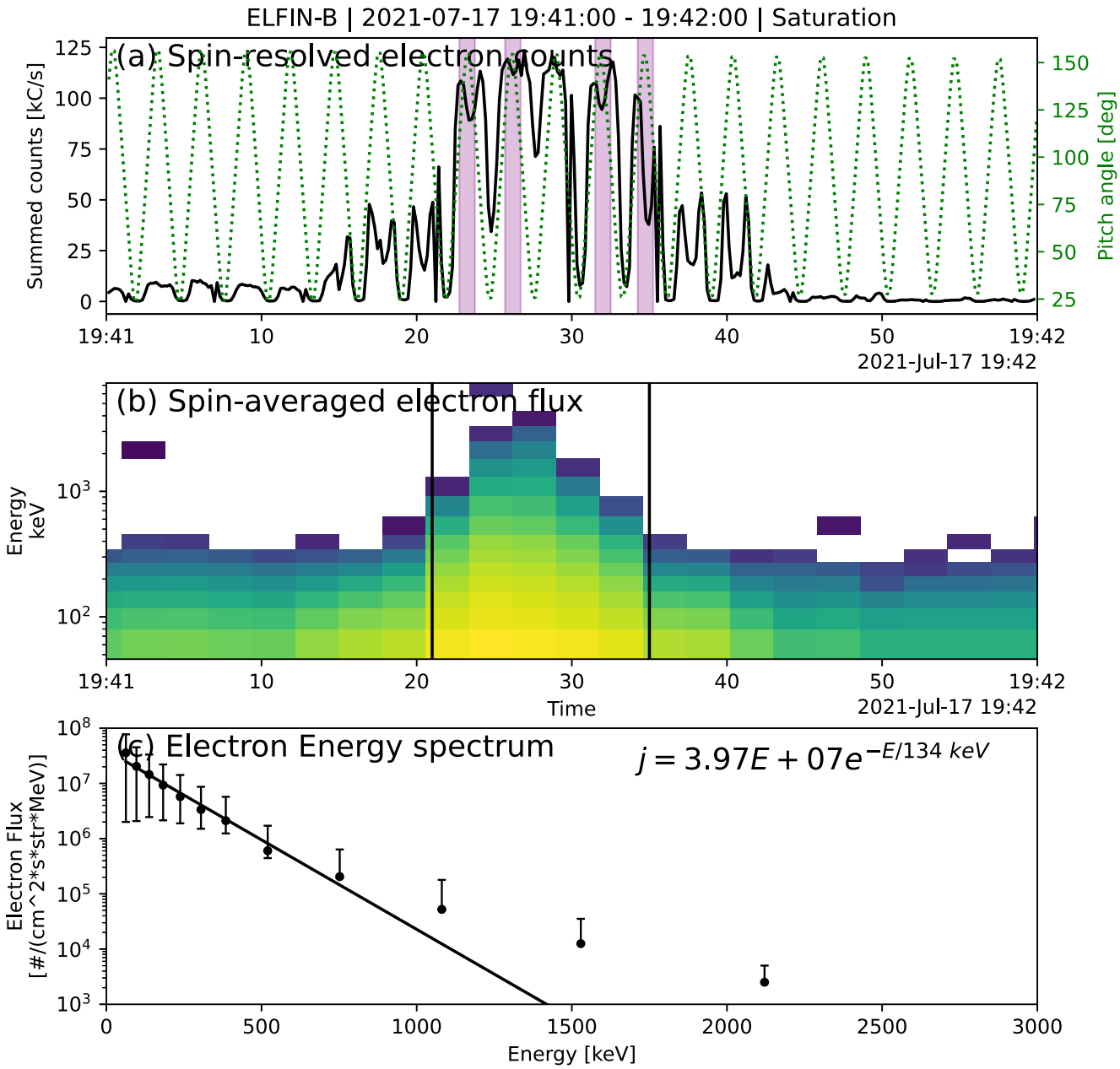

Figure A1. ELFIN-EPD electron data shows saturation during the PS burst. Panel (a) shows the spin resolved counts from all energy channels in black, every 270 ms, and the oscillating dotted green line is the local pitch angle of the instrument boresight. The purple bars indicate times when EPD scanned the center of the loss cone (centered on 180° pitch angles) and the count rates sagged, indicating that the instrument was beginning to saturate. Panel (b) is the omnidirectional electron flux in the same format as Figure 1a2 for fluxes with corresponding count rates > 3. Panel (c) shows the electron spectrum, fit to a similar energy range as MMS-FEEPS, with the error bars representing the inter-quartile range of the fluxes at each energy. The spectrum was derived using the time range bounded by the vertical black lines in Panel (b), and fit with an exponential function.

Assuming Poisson count distribution, and the aforementioned count summing condition, the detected count rates are related to the true count rate by:

$$R_{E,obs} = R_{E,true} e^{(R_E/R_\tau)} \tag{A1}$$

where $R_{E,obs}$ are the observed count rates summed over energy channel E and those above it, $R_{E,true}$ is the true count rate, and R_τ is the reciprocal of the dead time $\tau = 2.4$ μs/count. The solution to $R_{E,true}$ is given by the lower

real branch (argument $> -1/e$) of the Lambert W function (Corless et al., 1996) for all non-zero count energy channels.

This procedure always results in a monotonically decreasing number flux spectrum for channels with non-zero counts. This may potentially average out any energy-localized structure in the spectral slope, although such features are not the focus of this study.

Conflict of Interest

The authors declare no conflicts of interest relevant to this study.

Availability Statement

Both the ELFIN and MMS data used for this study are publicly available at https://data.elfin.ucla.edu/ and https://lasp.colorado.edu/mms/sdc/public/about/browse-wrapper/. We analyzed the MMS data using the Python library pyspedas (Angelopoulos et al., 2019) version 1.5.6 that is archived at https://pypi.org/project/pyspedas/ and https://github.com/spedas/pyspedas.

Acknowledgments
We are thankful for the countless engineers, technicians, scientists, and students who made the MMS and ELFIN missions a resounding success. M. Shumko, I.J. Cohen, and S. Raptis were supported by the Magnetospheric Multiscale (MMS) mission of NASA's Science Directorate Heliophysics Division via subcontract to the Southwest Research Institute (NNG04EB99C). G.K. Stephens was supported by NASA Grant 80NSSC24K0556. Lastly, this material is based upon work supported by the National Science Foundation under a Geospace Environment Modeling Grant (2225613).

References

Akasofu, S.-I. (1964). The development of the auroral substorm. *Planetary and Space Science*, *12*(4), 273–282. https://doi.org/10.1016/0032-0633(64)90151-5

Alken, P., Thébault, E., Beggan, C. D., Amit, H., Aubert, J., Baerenzung, J., et al. (2021). International geomagnetic reference field: The thirteenth generation. *Earth Planets and Space*, *73*, 1–25. https://doi.org/10.1186/s40623-020-01288-x

Angelopoulos, V. (2010). The ARTEMIS Mission. In *The ARTEMIS Mission* (pp. 3–25). Springer. https://doi.org/10.1007/978-1-4614-9554-3_2

Angelopoulos, V., Cruce, P., Drozdov, A., Grimes, E., Hatzigeorgiu, N., King, D., et al. (2019). The space physics environment data analysis system (SPEDAS). *Space Science Reviews*, *215*, 1–46. https://doi.org/10.1007/s11214-018-0576-4

Angelopoulos, V., Tsai, E., Bingley, L., Shaffer, C., Turner, D., Runov, A., et al. (2020). The ELFIN mission. *Space Science Reviews*, *216*(5), 1–45. https://doi.org/10.1007/s11214-020-00721-7

Angelopoulos, V., Zhang, X.-J., Artemyev, A., Mourenas, D., Tsai, E., Wilkins, C., et al. (2023). Energetic electron precipitation driven by electromagnetic ion cyclotron waves from ELFIN's low altitude perspective. *Space Science Reviews*, *219*(5), 37. https://doi.org/10.1007/s11214-023-00984-w

Artemyev, A., Angelopoulos, V., Zhang, X.-J., Chen, L., & Runov, A. (2023). Dispersed relativistic electron precipitation patterns between the ion and electron isotropy boundaries. *Journal of Geophysical Research: Space Physics*, *128*(12), e2023JA032200. https://doi.org/10.1029/2023ja032200

Artemyev, A., Angelopoulos, V., Zhang, X.-J., Runov, A., Petrukovich, A., Nakamura, R., et al. (2022). Thinning of the magnetotail current sheet inferred from low-altitude observations of energetic electrons. *Journal of Geophysical Research: Space Physics*, *127*(10), e2022JA030705. https://doi.org/10.1029/2022ja030705

Artemyev, A., Demekhov, A., Zhang, X.-J., Angelopoulos, V., Mourenas, D., Fedorenko, Y. V., et al. (2021). Role of ducting in relativistic electron loss by whistler-mode wave scattering. *Journal of Geophysical Research: Space Physics*, *126*(11), e2021JA029851. https://doi.org/10.1029/2021ja029851

Baker, D., Mason, G., Figueroa, O., Colon, G., Watzin, J., & Aleman, R. (1993). An overview of the solar anomalous, and magnetospheric particle explorer (SAMPEX) mission. *IEEE Transactions on Geoscience and Remote Sensing*, *31*(3), 531–541. https://doi.org/10.1109/36.225519

Birn, J., Hesse, M., Nakamura, R., & Zaharia, S. (2013). Particle acceleration in dipolarization events. *Journal of Geophysical Research: Space Physics*, *118*(5), 1960–1971. https://doi.org/10.1002/jgra.50132

Birn, J., Runov, A., & Hesse, M. (2014). Energetic electrons in dipolarization events: Spatial properties and anisotropy. *Journal of Geophysical Research: Space Physics*, *119*(5), 3604–3616. https://doi.org/10.1002/2013ja019738

Blake, J., Looper, M., Baker, D., Nakamura, R., Klecker, B., & Hovestadt, D. (1996). New high temporal and spatial resolution measurements by SAMPEX of the precipitation of relativistic electrons. *Advances in Space Research*, *18*(8), 171–186. https://doi.org/10.1016/0273-1177(95)00969-8

Blake, J., Mauk, B., Baker, D., Carranza, P., Clemmons, J., Craft, J., et al. (2016). The fly's eye energetic particle spectrometer (FEEPS) sensors for the magnetospheric multiscale (MMS) mission. *Space Science Reviews*, *199*(1–4), 309–329. https://doi.org/10.1007/s11214-015-0163-x

Blum, L., Li, X., & Denton, M. (2015). Rapid MeV electron precipitation as observed by SAMPEX/HILT during high-speed stream-driven storms. *Journal of Geophysical Research: Space Physics*, *120*(5), 3783–3794. https://doi.org/10.1002/2014ja020633

Brown, J. W., & Stone, E. C. (1972). High-energy electron spikes at high latitudes. *Journal of Geophysical Research*, *77*(19), 3384–3396. https://doi.org/10.1029/JA077i019p03384

Burch, J., Moore, T., Torbert, R., & Giles, B.-H. (2016). Magnetospheric multiscale overview and science objectives. *Space Science Reviews*, *199*(1–4), 5–21. https://doi.org/10.1007/s11214-015-0164-9

Chepuri, S., Jaynes, A., Turner, D., Gabrielse, C., Cohen, I., Baker, D., et al. (2023). Testing adiabatic models of energetic electron acceleration at dipolarization fronts. *Frontiers in Astronomy and Space Sciences*, *10*, 1266412. https://doi.org/10.3389/fspas.2023.1266412

Corless, R. M., Gonnet, G. H., Hare, D. E., Jeffrey, D. J., & Knuth, D. E. (1996). On the Lambert W function. *Advances in Computational Mathematics*, *5*(1), 329–359.

Donovan, E. (2016). Coupling between the geomagnetic tail and the inner magnetosphere. In *Space weather fundamentals* (pp. 131–148). CRC Press.

Dungey, J. (1963). Interactions of solar plasma with the geomagnetic field. *Planetary and Space Science*, *10*, 233–237. https://doi.org/10.1016/0032-0633(63)90020-5

Fu, H., Grigorenko, E. E., Gabrielse, C., Liu, C., Lu, S., Hwang, K., et al. (2020). Magnetotail dipolarization fronts and particle acceleration: A review. *Science China Earth Sciences*, *63*(2), 235–256. https://doi.org/10.1007/s11430-019-9551-y

Gabrielse, C., Angelopoulos, V., Runov, A., & Turner, D. L. (2014). Statistical characteristics of particle injections throughout the equatorial magnetotail. *Journal of Geophysical Research: Space Physics*, *119*(4), 2512–2535. https://doi.org/10.1002/2013ja019638

Gabrielse, C., Gkioulidou, M., Merkin, S., Malaspina, D., Turner, D. L., Chen, M. W., et al. (2023). Mesoscale phenomena and their contribution to the global response: A focus on the magnetotail transition region and magnetosphere-ionosphere coupling. *Frontiers in Astronomy and Space Sciences*, *10*, 1151339. https://doi.org/10.3389/fspas.2023.1151339

Gjerloev, J. (2009). A global ground-based magnetometer initiative. *Eos, Transactions American Geophysical Union*, *90*(27), 230–231. https://doi.org/10.1029/2009eo270002

Halford, A., McGregor, S., Hudson, M., Millan, R., & Kress, B. (2016). Barrel observations of a solar energetic electron and solar energetic proton event. *Journal of Geophysical Research: Space Physics*, *121*(5), 4205–4216. https://doi.org/10.1002/2016ja022462

Khotyaintsev, Y. V., Graham, D. B., Norgren, C., & Vaivads, A. (2019). Collisionless magnetic reconnection and waves: Progress review. *Frontiers in Astronomy and Space Sciences*, *6*, 70. https://doi.org/10.3389/fspas.2019.00070

Kim, H.-J., Lee, D.-Y., Wolf, R., Bortnik, J., Kim, K.-C., Lyons, L., et al. (2021). Rapid injections of MeV electrons and extremely fast step-like outer radiation belt enhancements. *Geophysical Research Letters*, *48*(9), e2021GL093151. https://doi.org/10.1029/2021gl093151

Kivelson, M. G., & Russell, C. T. (1995). *Introduction to space physics*. Cambridge University Press.

Lejosne, S., & Kollmann, P. (2020). Radiation belt radial diffusion at Earth and beyond. *Space Science Reviews*, *216*(1), 19. https://doi.org/10.1007/s11214-020-0642-6

Li, X. (2024). Unveiling energetic particle dynamics in the near-Earth environment from CubeSat missions. *AGU Advances*, *5*(3), e2024AV001256. https://doi.org/10.1029/2024av001256

Oka, M., Birn, J., Egedal, J., Guo, F., Ergun, R. E., Turner, D. L., et al. (2023). Particle acceleration by magnetic reconnection in geospace. *Space Science Reviews*, *219*(8), 75. https://doi.org/10.1007/s11214-023-01011-8

Pollock, C., Moore, T., Jacques, A., Burch, J., Gliese, U., Saito, Y., et al. (2016). Fast plasma investigation for magnetospheric multiscale. *Space Science Reviews*, *199*(1–4), 331–406. https://doi.org/10.1007/s11214-016-0245-4

Retzler, J., & Simpson, J. (1969). Relativistic electrons confined within the neutral sheet of the geomagnetic tail. *Journal of Geophysical Research*, *74*(9), 2149–2160. https://doi.org/10.1029/ja074i009p02149

Richardson, I., Owen, C., & Slavin, J. (1996). Energetic (>0.2 MeV) electron bursts in the deep geomagnetic tail observed by the Goddard Space Flight Center Experiment on ISEE 3: Association with geomagnetic substorms. *Journal of Geophysical Research*, *101*(A2), 2723–2740. https://doi.org/10.1029/95ja03375

Richardson, I., Owen, C., Slavin, J., & Von Rosenvinge, T. (1993). Energetic (>0.2 MeV) electron bursts observed by ISEE 3 in the deep (<240 Re) geomagnetic tail. *Journal of Geophysical Research*, *98*(A8), 13441–13451. https://doi.org/10.1029/93ja00501

Ripoll, J.-F., Claudepierre, S., Ukhorskiy, A., Colpitts, C., Li, X., Fennell, J., & Crabtree, C. (2020). Particle dynamics in the Earth's radiation belts: Review of current research and open questions. *Journal of Geophysical Research: Space Physics*, *125*(5), e2019JA026735. https://doi.org/10.1029/2019ja026735

Sergeev, V., Sazhina, E., Tsyganenko, N., Lundblad, J., & Søraas, F. (1983). Pitch-angle scattering of energetic protons in the magnetotail current sheet as the dominant source of their isotropic precipitation into the nightside ionosphere. *Planetary and Space Science*, *31*(10), 1147–1155. https://doi.org/10.1016/0032-0633(83)90103-4

Shi, X., Stephens, G. K., Artemyev, A. V., Sitnov, M. I., & Angelopoulos, V. (2024). Picturing global substorm dynamics in the magnetotail using low-altitude ELFIN measurements and data mining-based magnetic field reconstructions. *Space Weather*, *22*(10), e2024SW004062. https://doi.org/10.1029/2024sw004062

Sitnov, M., Birn, J., Ferdousi, B., Gordeev, E., Khotyaintsev, Y., Merkin, V., et al. (2019). Explosive magnetotail activity. *Space Science Reviews*, *215*(4), 1–95. https://doi.org/10.1007/s11214-019-0599-5

Sitnov, M. I., Stephens, G. K., Tsyganenko, N. A., Miyashita, Y., Merkin, V. G., Motoba, T., et al. (2019). Signatures of nonideal plasma evolution during substorms obtained by mining multimission magnetometer data. *Journal of Geophysical Research: Space Physics*, *124*(11), 8427–8456. https://doi.org/10.1029/2019ja027037

Sorathia, K., Michael, A., Merkin, V. G., Ukhorskiy, A. Y., Turner, D. L., Lyon, J., et al. (2021). The role of mesoscale plasma sheet dynamics in ring current formation. *Frontiers in Astronomy and Space Sciences*, *8*, 761875. https://doi.org/10.3389/fspas.2021.761875

Sorathia, K., Shumko, M., Liang, J., Arnold, H., Sinha, G., Merkin, V., et al. (2025). Direct radiation belt injections and their auroral counterparts. *Authorea Preprints*. https://doi.org/10.22541/essoar.175034878.82873768/v1

Sorathia, K. A., Ukhorskiy, A. Y., Merkin, V. G., Fennell, J. F., & Claudepierre, S. G. (2018). Modeling the depletion and recovery of the outer radiation belt during a geomagnetic storm: Combined MHD and test particle simulations. *Journal of Geophysical Research: Space Physics*, *123*(7), 5590–5609. https://doi.org/10.1029/2018ja025506

Stephens, G., Sitnov, M., Korth, H., Tsyganenko, N., Ohtani, S., Gkioulidou, M., & Ukhorskiy, A. (2019). Global empirical picture of magnetospheric substorms inferred from multimission magnetometer data. *Journal of Geophysical Research: Space Physics*, *124*(2), 1085–1110. https://doi.org/10.1029/2018ja025843

Sun, W., Oka, M., Øieroset, M., Turner, D. L., Phan, T., Cohen, I. J., et al. (2025). Relativistic electron acceleration and the "ankle" spectral feature in Earth's magnetotail reconnection. *The Astrophysical Journal Letters*, *978*(2), L28. https://doi.org/10.3847/2041-8213/ad9bb2

Terasawa, T., & Nishida, A. (1976). Simultaneous observations of relativistic electron bursts and neutral-line signatures in the magnetotail. *Planetary and Space Science*, *24*(9), 855–866. https://doi.org/10.1016/0032-0633(76)90076-3

Torbert, R., Russell, C., Magnes, W., Ergun, R., Lindqvist, P.-A., LeContel, O., et al. (2016). The fields instrument suite on mms: Scientific objectives, measurements, and data products. *Space Science Reviews*, *199*(1–4), 105–135. https://doi.org/10.1007/s11214-014-0109-8

Tsai, E., Palla, A., Norris, A., King, J., Russell, C., Ye, S., et al. (2024). Remote sensing of electron precipitation mechanisms enabled by ELFIN mission operations and ADCS. *Advances in Space Research*, *75*(9), 6706–6733. https://doi.org/10.1016/j.asr.2024.07.008

Turner, D. L., Cohen, I. J., Michael, A., Sorathia, K., Merkin, S., Mauk, B. H., et al. (2021). Can Earth's magnetotail plasma sheet produce a source of relativistic electrons for the radiation belts? *Geophysical Research Letters*, *48*(21), e2021GL095495. https://doi.org/10.1029/2021gl095495

Turner, D. L., Fennell, J., Blake, J., Clemmons, J., Mauk, B., Cohen, I., et al. (2016). Energy limits of electron acceleration in the plasma sheet during substorms: A case study with the magnetospheric multiscale (MMS) mission. *Geophysical Research Letters*, *43*(15), 7785–7794. https://doi.org/10.1002/2016gl069691

Ukhorskiy, A. Y., Sorathia, K. A., Merkin, V. G., Crabtree, C., Fletcher, A. C., Malaspina, D. M., & Schwartz, S. J. (2022). Cross-scale energy cascade powered by magnetospheric convection. *Scientific Reports*, *12*(1), 4446. https://doi.org/10.1038/s41598-022-08038-x

Usman, S., & Patil, A. (2018). Radiation detector deadtime and pile up: A review of the status of science. *Nuclear Engineering and Technology*, *50*(7), 1006–1016. https://doi.org/10.1016/j.net.2018.06.014

Wilkins, C., Angelopoulos, V., Runov, A., Artemyev, A., Zhang, X.-J., Liu, J., & Tsai, E. (2023). Statistical characteristics of the electron isotropy boundary. *Journal of Geophysical Research: Space Physics*, *128*(10), e2023JA031774. https://doi.org/10.1029/2023ja031774

Wiltberger, M., Merkin, V., Lyon, J., & Ohtani, S. (2015). High-resolution global magnetohydrodynamic simulation of bursty bulk flows. *Journal of Geophysical Research: Space Physics*, *120*(6), 4555–4566. https://doi.org/10.1002/2015ja021080

Zhang, X.-J., Artemyev, A., Angelopoulos, V., Tsai, E., Wilkins, C., Kasahara, S., et al. (2022). Superfast precipitation of energetic electrons in the radiation belts of the Earth. *Nature Communications*, *13*(1), 1611. https://doi.org/10.1038/s41467-022-29291-8

Zhang, X.-J., Artemyev, A. V., Li, X., Arnold, H., Angelopoulos, V., Turner, D. L., et al. (2025). Relativistic and ultra-relativistic electron bursts in Earth's magnetotail observed by low-altitude satellites. *Geophysical Research Letters*, *52*(2), e2024GL113280. https://doi.org/10.1029/2024GL113280

Zou, Y., Zhang, X.-J., Artemyev, A. V., Shen, Y., & Angelopoulos, V. (2024). The key role of magnetic curvature scattering in energetic electron precipitation during substorms. *Geophysical Research Letters*, *51*(14), e2024GL109227. https://doi.org/10.1029/2024gl109227